



A practical silver nanoparticle-based adsorbent for the removal of Hg^{2+} from water

E. Sumesh¹, M.S. Bootharaju¹, Anshup, T. Pradeep*

DST Unit of Nanoscience, Department of Chemistry and Sophisticated Analytical Instrument Facility, Indian Institute of Technology Madras, Chennai 600 036, India

ARTICLE INFO

Article history:

Received 11 December 2010

Received in revised form 16 February 2011

Accepted 17 February 2011

Available online 24 February 2011

Keywords:

Silver nanoparticles

Mercuric ions

Alumina

Reduction

Complexation

ABSTRACT

In this work, we describe the use of silver nanoparticles of 9 ± 2 and 20 ± 5 nm core diameter, protected by mercaptosuccinic acid (MSA) and supported on activated alumina for the removal of mercuric ions present in contaminated waters, at room temperature (28 ± 1 °C). These two nanoparticle samples were prepared by using two Ag:MSA ratios 1:6 and 1:3, respectively, during synthesis and were loaded on alumina at 0.5 and 0.3% by weight. The mechanism of interaction of silver nanoparticles with Hg^{2+} ions was studied using various analytical techniques such as ultraviolet–visible spectroscopy (UV–vis), Fourier transform infrared spectroscopy (FT–IR), X-ray diffraction (XRD), scanning electron microscopy (SEM), dynamic light scattering (DLS), inductively coupled plasma–optical emission spectrometry (ICP–OES), energy dispersive analysis of X-rays (EDAX), transmission electron microscopy (TEM) and X-ray photoelectron spectroscopy (XPS). Interactions of the metal ion with the metal core, the surface head group and the monolayer functionality were investigated. A high removal ability of 0.8 g of mercury per gram of Ag@MSA was achieved in the case of 1:6 Ag@MSA. These two materials show better uptake capacity of Hg^{2+} in the pH range of 5–6. The ease of synthesis of the nanomaterial by wet chemistry, capability to load on suitable substrates to create stable materials and affordable cost will make it possible to use this approach in field applications, especially for the treatment of Hg^{2+} contaminated waters.

© 2011 Elsevier B.V. All rights reserved.

1. Introduction

Water pollution is undoubtedly one of the major problems faced by the world today. Metals such as Hg, Pb, Cr, Cd, As in diverse forms constitute some of the major inorganic pollutants and have many harmful effects on humans and environment. Mercury is a highly toxic metal that is used widely despite its high levels of toxicity even at low dosages. Mercury enters air by natural and anthropogenic sources [1,2]. Mercury is a neurotoxin and the foetal nervous system is most vulnerable in this respect. Mercury exists in three chemical forms, namely elemental (Hg^0), inorganic mercurous and mercuric forms (Hg^{+1} and Hg^{+2}) and organic alkyl mercury. Methyl mercury and dimethyl mercury are the most toxic and stable forms of organomercury. Effects of mercury toxicity have been catalogued [3]. Due to the high toxicity effects, World Health Organization (WHO) has set the limit of mercury in drinking water as 0.001 mg/L. The permissible limit of mercury set by Indian standards for effluent discharge is 0.01 mg/L [4]. Mercury contamination in India is increasing at a shocking rate mainly due to the release of mercury-bearing industrial effluents ranging from 0.058 to 0.268 mg/L. In

India, chlor-alkali industries are the most important consumers of mercury and those located on river basins in eastern India are said to have released 60–320 times more mercury than the permissible limit, thereby polluting the river waters [5].

Some of the methods commonly employed for the treatment of mercury-contaminated waters are precipitation, membrane filtration and bioremediation [6]. These methods are costly and require skilled labor. Low cost and less maintenance makes adsorption a relatively better technique especially for small-scale treatment and as a polishing technique in large scale [7]. Metal based adsorbent systems such as zero-valent iron has caught large attention for its efficiency and practical applicability on a wide range of contaminants such as dehalogenation of halocarbons using fine grained iron [8]. The standard reduction potential of iron (-0.44 V) makes it more favorable for the reductive dehalogenation of alkyl halides ($\text{RX} + 2\text{e}^- + \text{H}^+ \rightarrow \text{RH} + \text{X}^-$) which ranges from 0.5 to 1.5 V, at pH 7. Many other metals along with iron such as zinc, copper and aluminium to improve the rate of reduction were tried [9]. Some other reactive metals such as magnesium [10] and zinc [11] were also experimented for dehalogenation. Zero valent iron is known for a process called cementation in engineering literature, which is the extraction of metals from low-grade ores. Here, it is known for its capability of reducing Cu^{2+} , Hg^{2+} and Ag^+ to metallic form [12]. Several materials containing iron such as iron sulfide, iron-bearing oxyhydroxides and aluminosilicate minerals were proved

* Corresponding author. Tel.: +91 44 2257 4208; fax: +91 44 2257 0545.

E-mail address: pradeep@iitm.ac.in (T. Pradeep).

¹ These authors have contributed equally.

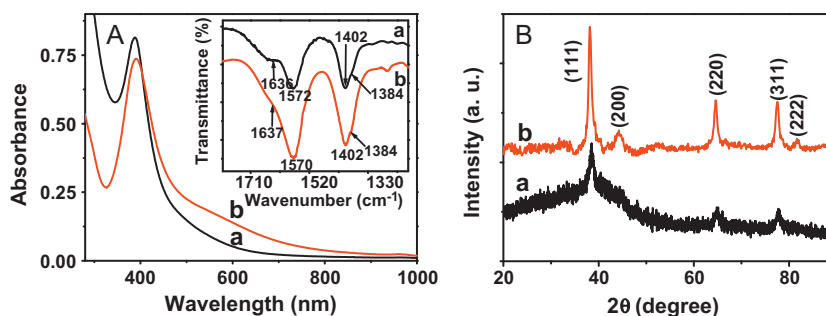


Fig. 1. UV-vis absorption spectra (A) and X-ray diffraction patterns (B) of 1:6 and 1:3 Ag@MSA nanoparticles (traces 'a' and 'b', respectively). Inset 'A' is the FT-IR spectra of both Ag@MSA nanoparticles (a and b) in the carboxylate region.

successful for the reduction and precipitation of metal ions. Out of all the iron based materials, elemental iron was found to be most successful for ground water remediation [13]. With the advent of nanotechnology, iron nanoparticles replaced the use of bulk iron based systems for the purification of water [14]. Surprisingly, after a few years, noble metal nanoparticles were also found to degrade halocarbons by the same mechanism of reductive dehalogenation [15–18]. In a report by Lisha et al., Hg^{2+} ions were reduced to zero-valent state, followed by the alloying of reduced mercury on gold nanoparticle surface [19]. We have examined the removal of other toxic species from water using nanomaterials [20–22].

Several studies on the interaction of silver nanoparticles and mercuric ions have been reported [23–25]. This is the first study of size dependent interaction of Ag@MSA nanoparticles with Hg^{2+} ions at different concentrations. In the present work, silver nanoparticle system is used for the sequestration of Hg^{2+} from water at room temperature (28 ± 1 °C). Since the reduction potential of silver ($\text{Ag}^+ + e^- \rightarrow \text{Ag}$, $E^0 = 0.80$ V) is comparable to that of mercury ($\text{Hg}^{2+} + 2e^- \rightarrow \text{Hg}$, $E^0 = 0.85$ V), we cannot expect high reactivity of Hg^{2+} with bulk silver. But, nanoscale silver is expected to be more reactive since there is a decrease in reduction potential upon decreasing the size [26]. The surface chemistry and optical properties of unprotected colloidal silver upon interaction with various metal ions have been investigated already [27]. Among the several ions such as Cd^{2+} , Ni^{2+} , Ag^+ and Hg^{2+} , the last one alone was found to get reduced along with partial oxidation of silver. The aim of the present work is to develop an efficient and reliable silver nanoparticle-based system for the removal of Hg^{2+} from water. Two different systems with MSA as the ligand were studied, namely 1:3 Ag@MSA and 1:6 Ag@MSA (the ratio refers to the molar ratio of silver to MSA used in the sample preparation). The nanoparticles were used in the supported and unsupported forms. We chose this system as the synthesis of these particles is possible in water:methanol mixtures and their purification is easy. They can be easily loaded on supports to create a practical solution even with limited resources, in rural settings. The reactants and products were analyzed by various analytical techniques for understanding the mechanism of interaction. Finally, the practical applicability of this system was checked by a column experiment. It is important to note that monolayer protected nanoparticles, synthesized in water:methanol medium, are used in the study and it is shown that both the metal core and the monolayer are important in the removal mechanism.

2. Experimental

Silver nanoparticles protected with MSA were synthesized by the reduction of AgNO_3 using NaBH_4 [28]. The details of the nanoparticles synthesis, batch experiments of Hg^{2+} and Ag@MSA particles, loading of Ag@MSA particles on alumina and column

experiments are described in [Supplementary data 1](#). The instrumentation part is given in [Supplementary data 2](#).

3. Results and discussion

3.1. Characterization of Ag@MSA nanoparticles

The plasmon absorption of silver nanoparticles appears around 390–400 nm. Although the peak positions of 1:3 and 1:6 Ag@MSA are almost the same (Fig. 1A), the surface plasmon of 1:6 Ag@MSA shows a sharp feature when compared to that of 1:3 Ag@MSA, which shows a broader line shape with a high wavelength shoulder. It can be assumed from this that the 1:3 Ag@MSA sample has a larger particle size distribution. This is supported by XRD measurements also (Fig. 1B). The pristine silver nanoparticles of both 1:6 and 1:3 ratios showed all the peaks corresponding to metallic silver [29]. In 1:3 sample (trace b) silver features are sharp whereas in 1:6 sample (trace a), silver features are broadened. This supports the small size and amorphous nature of the 1:6 sample. The FT-IR spectra of both the samples are shown in Fig. S3 (Supplementary data). It showed that the S–H stretching peak present in pure MSA at 2548 cm^{-1} is absent in Ag@MSA. The broad peak centered at 3418 cm^{-1} is due to the O–H stretching, due to the presence of water molecules in the particles. The expanded region of carboxylate group is shown as inset of Fig. 1A. Two sharp and strong peaks are present at 1572 and 1402 cm^{-1} , due to asymmetric and symmetric vibrations of the carboxylate group. A shoulder at 1384 cm^{-1} is also seen which is also due to the symmetric stretching of carboxylate [30]. These features suggest the existence of MSA as carboxylate ions on the nanoparticles. The differences (Δ) between asymmetric and symmetric modes of carboxylates in parent Ag@MSA (both 1:3 and 1:6) are 170 and 188 cm^{-1} . These Δ values fall in the region of bridging bidentate mode [31,32] of carboxylate of MSA. The 1:6 Ag@MSA particles are well-defined and spherical with an average particle size of $\sim 9 \text{ nm}$ (Fig. 2A and B). At this large Ag:S ratio, the size distribution is uniform. Particles are not crystalline as shown in the HRTEM image (Fig. 2B). The 1:3 Ag@MSA nanoparticles (Fig. 2C and D) are also spherical, but not as well defined and the size-distribution was not as narrow as in the former. Such particles show crystalline nature as shown in HRTEM (Fig. 2D). While most of the particles are below 15–17 nm, larger particles were also seen; this distribution is typical of silver nanoparticles.

3.2. Uptake of Hg^{2+} by Ag@MSA loaded on alumina

3.2.1. Effect of pH

In this study, 30 mg alumina loaded 1:6 Ag@MSA nanoparticles were treated with 30 mL of 2 ppm Hg^{2+} solutions. The pH of the solution was adjusted to the required value by using 0.1 M HCl and 0.1 M NaOH solutions. The pH values were 2, 5, 7, 9 and 12.

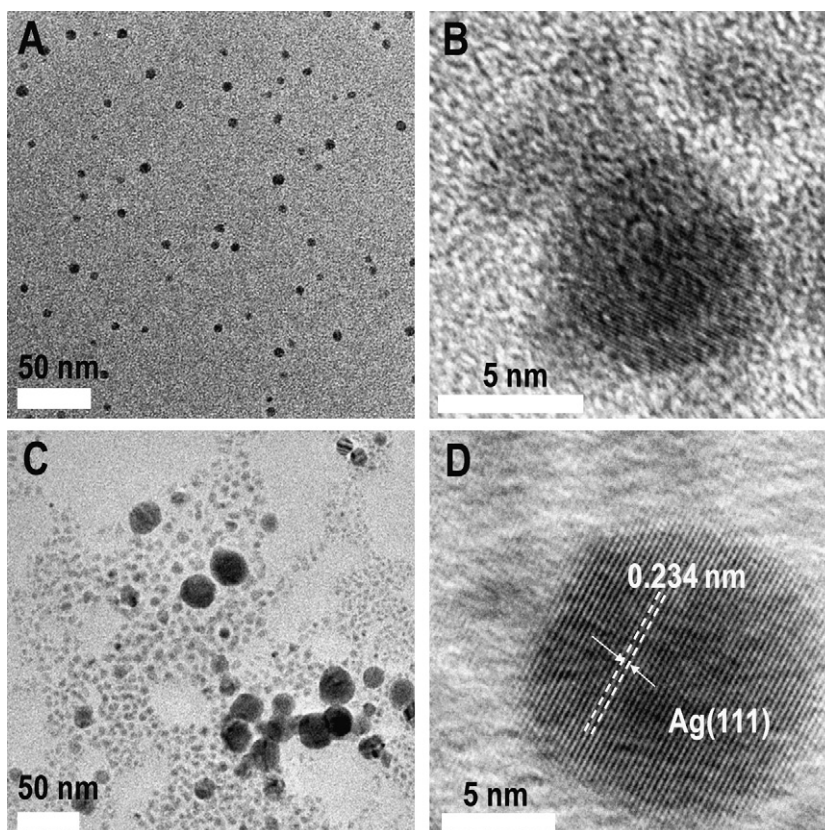


Fig. 2. TEM images of 1:6, 1:3 Ag@MSA nanoparticles (A and C, respectively). A and C are large area images and B and D are single nanoparticles. In B (1:6 Ag@MSA) no lattice is seen while in D (1:3 Ag@MSA) the lattice observed is marked.

These solutions were shaken with a shaker for 24 h and Hg^{2+} in solutions were analyzed afterwards with UV–vis absorption spectroscopy using the Rhodamine 6G method [33]. The concentration of Hg^{2+} in the solution was obtained from the calibration plot (Fig. S4). A straight line is obtained by plotting the concentrations of standard mercury solutions (0.0, 0.5, 1.0, 1.5 and 2.0 ppm) and the absorbance of Hg^{2+} –Rhodamine 6G complex at 575 nm. Similar study was done with alumina loaded 1:3 Ag@MSA nanoparticles also and the results are shown in Fig. 3. The percentage of removal by both the systems is high at pH 5–6 and it is decreasing with increase of pH. The reason for the decrease of uptake capacity at higher pH may be that Hg^{2+} forms stable mercuric hydroxo complexes with high $\log K=22$ which may not interact with nanoparticles surface [34]. Among these two materials, 1:6 Ag@MSA showed better performance than 1:3 Ag@MSA.

3.2.2. Effect of other ions

The effect of other ions like Ca^{2+} , Mg^{2+} , Cl^- , NO_3^- , SO_4^{2-} etc. on the uptake of 2 ppm Hg^{2+} present in normal tap water by alumina loaded 1:6 and 1:3 Ag@MSA was also studied. In this study, 30 mg of each material and 30 mL of 2 ppm Hg^{2+} solutions prepared in normal tap water were used. The pH of the normal tap water was found to be 8. The Hg^{2+} present in solutions was analyzed after a day with UV–vis absorption spectroscopy. The mercury removal percentages by alumina loaded 1:6 and 1:3 materials were 68 and 46%, respectively. This shows that effect of other ions on the uptake of Hg^{2+} is considerable in both the materials.

3.2.3. Column studies

We conducted an experiment (as described in Supplementary data 1) in which the capacities of three adsorbent systems (pure alumina, 1:3 and 1:6 Ag@MSA loaded on alumina) were compared.

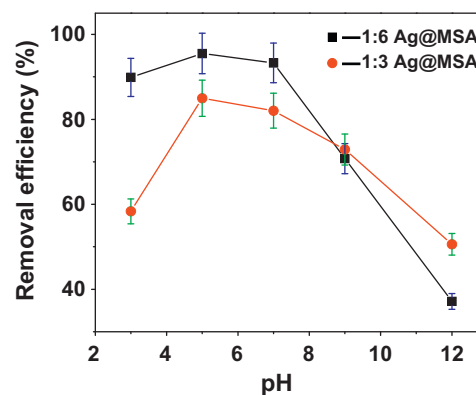


Fig. 3. A plot of the pH of Hg^{2+} solutions and removal efficiency of alumina loaded 1:6 and 1:3 Ag@MSA nanoparticles.

The adsorbent samples were chosen such that the amounts of silver in the last two were the same. The ICP–OES data are shown in Fig. 4. The solutions were collected up to 4.0 and 6.5 L in the case of 1:3 and 1:6 Ag@MSA, respectively. The breakthrough is observed after passing 2.0 and 5.5 L Hg^{2+} in the case of 1:3 and 1:6 Ag@MSA, respectively. We have ascertained that the Hg^{2+} concentration goes below 85 ppb (in 1:6 Ag@MSA case) with an input concentration of 2 ppm. The amount of adsorbent or loading has to be increased in bringing the output concentrations to acceptable limits in practical applications. It may be noted that 2 ppm input is ten times higher than even the most contaminated waters. The output water from pure alumina column contains 1.7 ppm of Hg^{2+} after passing 200 mL, 2 ppm Hg^{2+} solution (Fig. S5A). This shows alumina alone cannot act as good adsorbent for mercury.

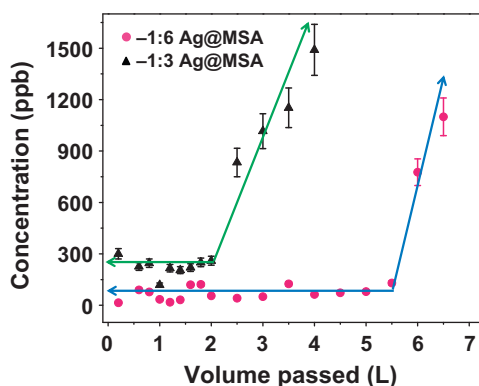


Fig. 4. A plot of the concentration of Hg^{2+} detected in ppb as a function of the volume of Hg^{2+} solution passed.

In order to understand the particle size effect in the interaction of Hg^{2+} ions with silver, AgNO_3 solution was directly reduced on the alumina surface using NaBH_4 , keeping the amount of silver the same as in the loaded samples. The same study was done using this material as adsorbent. Here, silver was present on alumina in the bulk form. The performance was comparable to that of bare alumina (Fig. S5B). This proves the importance of nanoscale materials in the observed phenomenon and shows that the reactivity of the nanoparticles is not lost even after loading on alumina.

There was no significant color change in the case of pure alumina adsorbent after passing Hg^{2+} solution through the column. The parent samples of 1:3 and 1:6 Ag@MSA were grey and beige, respectively. After the experiment, the darker regions may be due to the deposition of mercury on the column whereas pale regions may be the areas where etching of Ag had taken place (Fig. S6). When the color of the column was changed almost completely, the output water started showing the presence of mercury indicating that the column was getting exhausted. The visible color change of the column serves as a practical indicator.

The output solutions were tested for silver content with ICP-OES in the case of 1:6 sample and data are shown in Fig. S7. Initially as silver and mercuric ions are interacting and the output solution contains less silver. As the interaction proceeds, silver content starts increasing in the output water. Subsequently, silver content is decreased. This shows that the silver ions, which may be formed at the nanoparticle surface are entering into the solution. The decrease in concentration of Ag with time is not due to the complete removal of Ag from the adsorbent. Because of small size of Ag@MSA nanoparticles, some particles may be leaching. The other possibility is that if there exists some unwashed Ag@MSA on alumina which can come out. As time progresses, when all the excess nanoparticles came out, there is no silver detected.

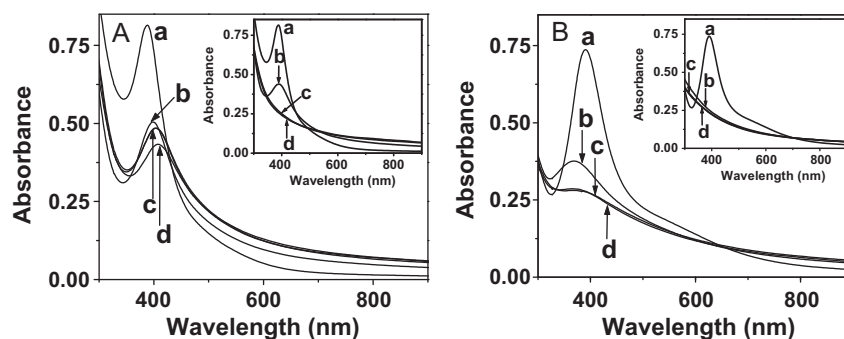


Fig. 5. The UV-vis spectra of the silver nanoparticle systems on the introduction of mercuric ions with time. A and B represent the time dependant spectrum of the interaction of 1:6 and 1:3 Ag@MSA nanoparticles, respectively, upon the introduction of 100 ppm Hg^{2+} . Inset shows the interaction with 250 ppm Hg^{2+} . (a) Pure silver nanoparticles, (b) silver nanoparticles in Hg^{2+} solution immediately after addition, (c) after 6 h and (d) after 24 h.

3.3. Mechanism explanation

The mechanism of interaction of Hg^{2+} with Ag@MSA nanoparticles is probed with several following spectroscopic and microscopic tools.

3.3.1. UV-vis spectroscopy

The plasmon band of silver nanoparticles is extremely sensitive to adsorption of nucleophiles and electrophiles on their surface [35]. The changes in the surface plasmon seem to be different in both the nanoparticle cases with concentration of Hg^{2+} . The lowest concentration data are presented in Fig. S8. Here, the plasmon absorption got red shifted and the broadening of the peak was noticed in both the cases. This may be due to the withdrawal of electron density from silver nanoparticles because of adsorption of cations on the surface of the particles [35]. There can also be aggregation as a result of this. On the contrary, at a medium concentration (100 ppm), there is a blue shift observed along with dampening for the 1:3 Ag@MSA sample alone (Fig. 5). The 1:6 Ag@MSA sample did not show any blue shift, a minor red shift was seen instead. Decrease in the intensity of the plasmon is more because much more Hg^{2+} ions are now in the solution. The blue shift and dampening can be due to the changes in the refractive index of the particles and change in composition due to the formation of an amalgam [35]. At a still higher concentration, the dampening of the intensity is more prominent. The peak disappears almost fully very fast and after that the curve remains almost the same. This is due to the near complete reaction of nanoparticles. This was noticed in TEM images also. Fig. S9A is large area TEM image of 1:6 Ag@MSA treated with 250 ppm Hg^{2+} in which the particles are aggregated. Fig. S9B is the HRTEM image of the same sample in which no individual particle is seen.

3.3.2. FT-IR analysis

After treating with 100 ppm Hg^{2+} solution, the carboxylate peaks at 1572, 1402 and 1384 cm^{-1} in 1:6 sample got shifted to 1581, 1394 and 1373 cm^{-1} , respectively [32]. The 1:3 sample also shows similar shifts (Fig. 6). In Hg^{2+} treated samples (both 1:3 and 1:6 Ag@MSA) the differences between symmetric and asymmetric modes of carboxylates are 187 and 208 cm^{-1} . The Δ value of 187 cm^{-1} fall in the bridging bidentate region and Δ of 208 cm^{-1} fall in the monodentate region [31,32]. The shift of carboxylate peak to the lower frequency corresponds to metal bound carboxylate and clearly indicates the interaction of carboxylate groups of MSA with Hg^{2+} ions. In the Hg^{2+} reacted sample, some of the carboxylates are present in bridging bidentate mode and some of them are present in the monodentate mode.

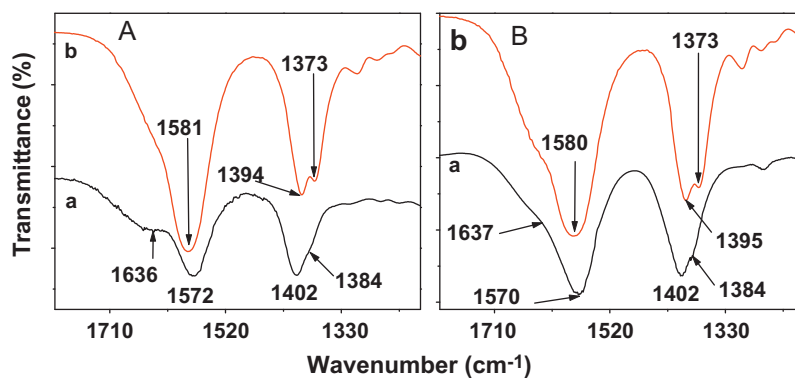


Fig. 6. FT-IR spectra of (A) 1:6 and (B) 1:3 Ag@MSA nanoparticles in the carboxylate region. Traces a and b correspond to the nanoparticles before and after treatment with 100 ppm Hg^{2+} solution, respectively.

3.3.3. DLS measurements

The average hydrodynamic diameters of pure 1:6 Ag@MSA, the particles treated with 0.1, 10 and 100 ppm Hg^{2+} solutions are 28.8, 43.6, 54.2 nm and 103.2 μm , respectively (Fig. S10). It shows the increase of particle size with Hg^{2+} concentration which is supported by UV–visible spectra. The silver plasmon peak got red shifted from 389 nm (in 1:6 Ag@MSA) to 398 and 419 nm in 0.1 and 10 ppm cases, respectively (Fig. S11). The plasmon peak was disappeared in 100 ppm solution indicate that all the nanoparticles were interacted with Hg^{2+} ions. Similar increase of the average hydrodynamic diameters and red shift of plasmon absorption of 1:3 Ag@MSA particles after treating with Hg^{2+} solutions are noticed (Figs. S10 and S11, respectively). In both the DLS plots, the particle size distribution after treating with mercuric ions was broad which is supported by broadening of the surface plasmon peaks of the nanoparticles. After adding 0.1, 10 and 100 ppm Hg^{2+} solutions, the pH was changed

from 8.1 to 7.7, 7.2 and 5.4, respectively. These changes were almost the same in both (1:6 and 1:3 Ag@MSA) systems. The change of pH from basic to neutral and acidic with increase of Hg^{2+} concentration show the interaction of Hg^{2+} with MSA carboxylate groups.

3.3.4. TEM images

Fig. 7 shows the TEM image of a structure formed by the addition of 100 ppm Hg^{2+} to the 1:6 Ag@MSA colloid, with the corresponding elemental maps. It shows mercury and silver in good amounts. The TEM image of an aggregated mass, formed after the addition of 25 ppm Hg^{2+} to the 1:3 Ag@MSA solution reveals a few distinctly visible nanoparticles too. This suggests that the agglomerated masses are formed by the fusion of independent silver nanoparticles (Fig. S12A). The TEM image of the agglomerated mass formed by the introduction of 100 ppm Hg^{2+} ions to 1:3 Ag@MSA colloid shows a sheet-like structure with a few micrometers in

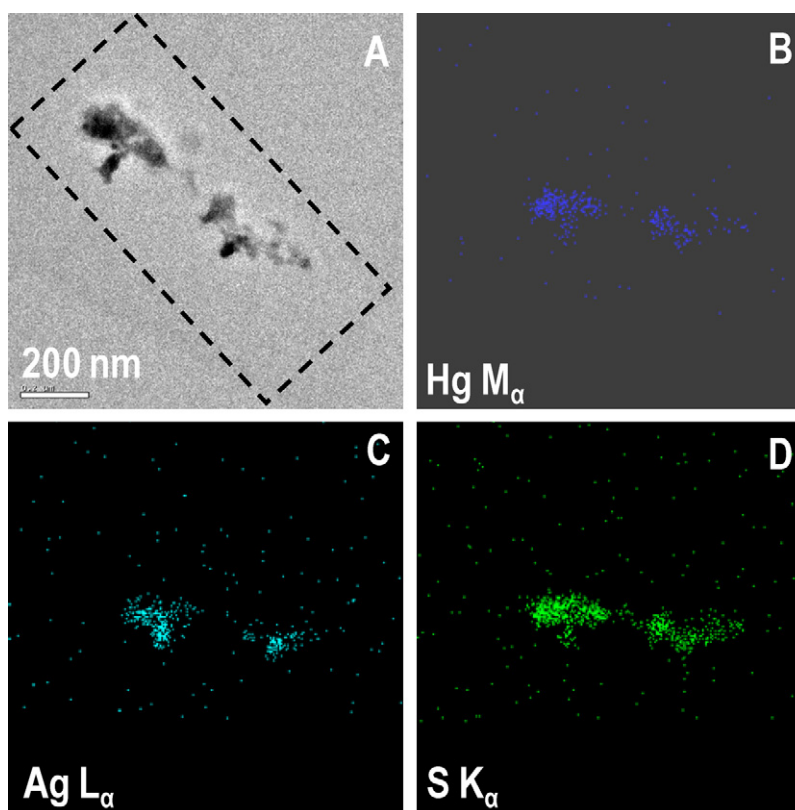


Fig. 7. The TEM and EDAX images of an aggregated mass formed by the reaction of 1:6 Ag@MSA with 100 ppm Hg^{2+} solution. (A) The TEM image. Elemental maps of (B) mercury, (C) silver and (D) sulphur. The elemental maps are tilted by about forty-five degrees with respect to the TEM image.

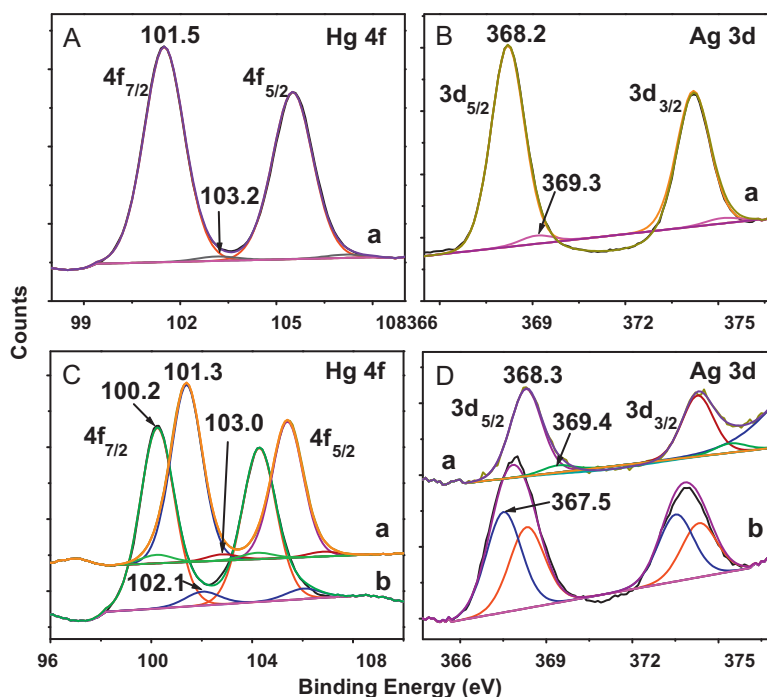


Fig. 8. XPS spectra of Hg 4f and Ag 3d regions from the residue obtained after the reaction with mercuric ions. (A) and (B) are of 1:6 Ag@MSA. (C) and (D) are of 1:3 Ag@MSA. (a) Residue obtained after the reaction with 100 ppm Hg^{2+} and (b) residue obtained after the reaction with 25 ppm Hg^{2+} .

dimension. On higher magnification, the lattice planes corresponding to paraschachnerite or Ag_3Hg_2 were visible in some areas, which is shown as inset (Fig. S12B). This also correspond to peaks in the XRD (see below). The composition of alloy (Ag_3Hg_2) is also supported by the EDAX quantification data of this sample which showed a composition of $\text{Ag}_{2.6}\text{Hg}_{2.0}$ (Fig. S13).

3.3.5. XRD data

The X-ray diffractograms of the residue formed when 100 ppm of Hg^{2+} solution treated with 1:3 and 1:6 Ag@MSA cases show that the silver features have disappeared. In the case of 1:3 Ag@MSA, two peaks (Fig. S14, trace b) corresponding to an Ag–Hg alloy were found. These match with the strongest peaks of Ag_3Hg_2 or paraschachnerite having an orthorhombic crystal structure [36]. Thus reduction of mercury may be inferred.

On the silver surface protected with monolayers, there can be different behaviors as a function of various concentrations. At low mercury concentrations, the cations are reduced to metallic state on the surface of silver nanoparticles and due to the low concentration, amalgam formation is less. At high concentrations, more mercury gets deposited. At moderate concentrations, Hg^{2+} ions get reduced on the surface of silver, forming a few overlayers of mercury which are strongly bound. Here, there is a good possibility of formation of alloy by the slow diffusion of mercury to the interior of silver particles. Several competing aspects are involved which determine the product formed.

3.3.6. XPS investigation

In Fig. S15, XPS survey spectra of pristine and Hg^{2+} treated nanoparticles (1:3 and 1:6 Ag@MSA) are shown. The presence of sodium is from sodium borohydride used as the reducing agent (in the synthesis of nanoparticles) and due to the fact that MSA is a dicarboxylic acid, which can be in the carboxylate form. Fig. 8A and B shows the XPS spectra of the 1:6 Ag@MSA nanoparticle residue obtained after the reaction with 100 ppm Hg^{2+} ions. The Hg $4f_{7/2}$ peak at 101.5 eV in Fig. 8A corresponds to mercuric ions bonded to carboxylate groups which match with the XPS of Hg-citrate [37].

The peak at 103.2 eV is due to the complexation of mercuric ions with carboxylate groups of MSA [37]. The reduction of Hg^{2+} ions is not observed in 1:6 Ag@MSA – 100 ppm Hg^{2+} system which may be due to more MSA in this system. This is supported by XRD also in which no alloy formation was observed. The presence of metallic silver (Ag $3d_{5/2}$ at 368.2 eV) is shown in Fig. 8B. The Ag $3d_{5/2}$ at 369.3 eV shows the bonded silver to the capping agent. Fig. 8C and D shows the XPS spectra of the 1:3 Ag@MSA nanoparticle residue obtained after the reaction with 25 and 100 ppm Hg^{2+} ions. The Hg $4f_{7/2}$ peak appearing at 100.2 eV in the case of 25 and 100 ppm Hg^{2+} solution corresponds to that of metallic mercury (1:3 Ag@MSA) [37]. This may be due to the reduction of mercuric ions by silver nanoparticles. This supports the alloy formation in 1:3 Ag@MSA – 100 ppm Hg^{2+} system. The reduction is more in the 25 ppm case which may be due to the availability of more silver content per mercuric ion.

As silver gives electrons for reduction, it undergoes oxidation forming silver oxide [38]. The Ag $3d_{5/2}$ at 367.5 eV corresponds to silver oxide and that at 368.3 eV corresponds to metallic silver (Fig. 8D). The BE shifts of the 3d peaks may be due to factors other than electronegativity differences such as lattice potential, work function changes, and extra-atomic relaxation energy reported earlier [38]. The peak at 369.4 eV is due to the silver bonded to the organic protecting agent [38,39]. When the concentration of Hg^{2+} was increased to 100 ppm, the Hg $4f_{7/2}$ was seen at higher binding energies such as 101.3 eV which can be due to bonded Hg^{2+} to the carboxylate groups or the formed Hg^+ ions on the surface of silver nanoparticles. The minor peaks seen at 102.1 and 103.0 eV can be due to the complexation of Hg^{2+} with the carboxylate groups of MSA [37]. The monolayer bound Hg^{2+} at 100 ppm concentration is in agreement with FT-IR data (Fig. 6).

The $\text{S} 2p_{3/2}$ at 162.3 eV after reaction with Hg^{2+} suggest the intact monolayer in all the samples treated with mercuric ions (Fig. 9) [40]. In the 1:3 sample, when treated with 25 ppm Hg^{2+} solution, $\text{S} 2p_{3/2}$ at 166.0 eV is seen suggesting the formation of sulphite attributed to aerial oxidation (Fig. 9C). The presence of C 1s at 286.3 (± 0.3), 288.1 (± 0.3) and 289.9 (± 0.3) eV correspond to carbon in dif-

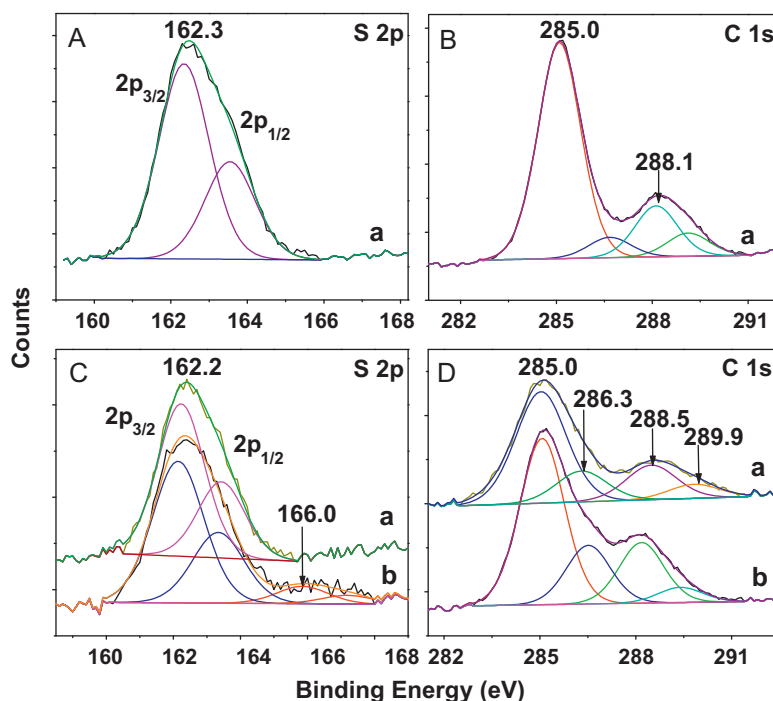


Fig. 9. The S 2p and C 1s peaks in the XPS spectra before and after the reaction of Hg^{2+} ions. (A) and (B) are for 1:6 Ag@MSA. (C) and (D) are for 1:3 Ag@MSA. (a) After reaction with 100 ppm Hg^{2+} and (b) after reaction with 25 ppm Hg^{2+} .

ferent chemical environments in both 1:3 and 1:6 samples treated with Hg^{2+} ions (Fig. 9) [41]. The peaks at 288.1 (± 0.3) and 289.9 (± 0.3) eV are attributed to the carboxylate carbons.

It can thus be suggested that there are two mechanisms by which the removal of Hg^{2+} ions is taking place. In 1:6 Ag@MSA case, at lower and higher concentrations, complexation/adsorption with carboxylate groups of MSA may occur. In 1:3 Ag@MSA case, at lower Hg^{2+} concentrations such as at 25 ppm, the ions interact with the nanoparticle core leading to reduction. At higher concentrations such as 100 ppm, the uptake may be occurring by reduction/adsorption.

The cost of removing mercury from water using the adsorbent composition reported here is quite competitive. Assuming an input concentration of 1 ppm Hg^{2+} , the cost of adsorbent works out to be \$5 per kL. Herein, the cost component for silver the salt is approximately 60%. Considering that silver loading on alumina can be up to 0.5%, the recovery of silver is commercially viable. Therefore, Ag@MSA loaded on alumina works out to be a commercially feasible option for large-scale mercury removal from water. Ag@MSA on alumina adsorbent shows manifold increased performance when compared to some of the conventional mercury adsorbents. The capacities of some of the known adsorbents for mercury removal are compared in Table S1 (Supplementary data). The commercially available adsorbents are listed in Table S2 (Supplementary data).

4. Conclusions

We have found that water soluble silver nanoparticles supported on alumina is an efficient system for the removal of mercuric ions from water. By comparing two different silver systems, we have demonstrated the effect of ligand concentration at the nanoparticle surface on the adsorption capacity. The mechanisms by which silver nanoparticles interact with mercuric ions was studied using UV–vis spectroscopy, FT-IR spectroscopy, DLS, ICP-OES, XRD, SEM, EDAX, TEM and XPS. A batch experiment using three different concentrations of mercuric solutions was done to understand the mechanism better. The mercuric ions get

removed by amalgamation and by complexation/adsorption. Practical implementation of this system is described by comparing the performance in column experiments using bare alumina and two different types of silver nanoparticles-loaded alumina. The residual mercury and silver were estimated in the output water using ICP-OES. Both the materials show better Hg^{2+} removing capacity in the 5–6 pH range. The 1:6 Ag@MSA loaded alumina showed a removal of 0.8 g per g of silver. This system appears to offer a practical solution for the purification of contaminated waters, although the effect of other ions is still significant. The results show that the reduced dimension and compatible monolayer enhance the Hg^{2+} scavenging capacity significantly.

Acknowledgements

We thank Department of Science and Technology, Government of India for constantly supporting our research program on nanomaterials. Dr. Balachandran Unni Nair and Mr. M. Nidhin, CLRI, Chennai, are acknowledged for the DLS measurements.

Appendix A. Supplementary data

Supplementary data associated with this article can be found, in the online version, at doi:10.1016/j.jhazmat.2011.02.061.

References

- [1] F. Zahir, S.J. Rizwi, S.K. Haq, R.H. Khan, Low dose mercury toxicity and human health, *Environ. Toxicol. Pharmacol.* 20 (2005) 351–360.
- [2] W.H. Schroeder, J. Munthe, Atmospheric mercury—an overview, *Atmos. Environ.* 32 (1998) 809–822.
- [3] P. Holmes, K.A.F. James, L.S. Levy, Is low-level environmental mercury exposure of concern to human health, *Sci. Total Environ.* 408 (2009) 171–182.
- [4] R.C. Srivastava, Guidance and Awareness Raising Materials under new UNEP Mercury Programs (Indian Scenario), Centre for Environmental Pollution Monitoring and Mitigation, India, 2004.
- [5] www.cseindia.org/node/439.
- [6] L.Y. Blue, M.A.V. Aelstyn, M. Matlock, D.A. Atwood, Low-level mercury removal from groundwater using a synthetic chelating ligand, *Water Res.* 42 (2008) 2025–2028.

- [7] Treatment technologies for mercury in soil, waste and water. <http://www.epa.gov/tio/download/remed/542r07003.pdf>. Accessed on 19/02/2010.
- [8] R.W. Gillham, S.F. O'Hannesin, Enhanced degradation of halogenated aliphatics by zero-valent iron, *Ground Water* 32 (1994) 958–967.
- [9] K.H. Sweeny, *AIChE Symp. Ser.* 77 (1981) 72–78.
- [10] J. Morales, R. Hutcheson, I.F. Cheng, Dechlorination of chlorinated phenols by catalyzed and uncatalyzed Fe(0) and Mg(0) particles, *J. Hazard. Mater.* 90 (2002) 97–108.
- [11] J.H. Choi, Y.H. Kim, Reduction of 2,4,6-trichlorophenol with zero-valent zinc and catalyzed zinc, *J. Hazard. Mater.* 166 (2009) 984–991.
- [12] K.J. Cantrell, D.I. Kaplan, T.W. Wietsma, Zero-valent iron for the in situ remediation of selected metals in groundwater, *J. Hazard. Mater.* 42 (1995) 201–212.
- [13] R.M. Powell, R.W. Puls, S.K. Hightower, D.A. Sabatini, Coupled iron corrosion and chromate reduction: mechanisms for subsurface remediation, *Environ. Sci. Technol.* 29 (1995) 1913–1922.
- [14] N. Savage, M. Diallo, J. Duncan, A. Street, R. Sustich (Eds.), *Nanotechnology Applications for Clean Water*, William Andrew, Norwich, NY, 2009, and the papers cited therein.
- [15] A.S. Nair, T. Pradeep, Halocarbon mineralization and catalytic destruction by metal nanoparticles, *Curr. Sci.* 84 (2003) 1560–1564.
- [16] A.S. Nair, T. Pradeep, Extraction of chlorpyrifos and malathion from water by metal Nanoparticles, *J. Nanosci. Nanotechnol.* 7 (2007) 1–7.
- [17] A.S. Nair, R.T. Tom, T. Pradeep, Detection and extraction of endosulfan by metal Nanoparticles, *J. Environ. Monit.* 5 (2003) 363–365.
- [18] Anshup, T. Pradeep, Noble metal nanoparticles for water purification: a critical review, *Thin Solid Films* 517 (2009) 6441–6478.
- [19] K.P. Lisha, Anshup, T. Pradeep, Towards a practical solution for removing inorganic mercury from drinking water using gold nanoparticles, *Gold Bull.* 42 (2009) 144–152.
- [20] S.M. Maliyekkal, K.R. Anshup, T. Antony, Pradeep, High yield combustion synthesis of nanomagnesia and its application for fluoride removal, *Sci. Total Environ.* 408 (2010) 2273–2282.
- [21] S.M. Maliyekkal, K.P. Lisha, T. Pradeep, A novel cellulose–manganese oxide hybrid material by in situ soft chemical synthesis and its application for the removal of Pb(II) from water, *J. Hazard. Mater.* 181 (2010) 986–995.
- [22] S.M. Maliyekkal, L. Philip, T. Pradeep, As(III) removal from drinking water using manganese oxide-coated-alumina: performance evaluation and mechanistic details of surface binding, *Chem. Eng. J.* 153 (2009) 101–107.
- [23] T. Morris, H. Copeland, E. McLinden, S. Wilson, G. Szulczewski, The effects of mercury adsorption on the optical response of size-selected gold and silver nanoparticles, *Langmuir* 18 (2002) 7261–7264.
- [24] L. Katsikas, M. Gutierrez, A. Henglein, Bimetallic colloids: silver and mercury, *J. Phys. Chem.* 100 (1996) 11203–11206.
- [25] Y. Fan, Z. Liu, L. Wang, J. Zhan, Synthesis of starch-stabilized Ag nanoparticles and Hg²⁺ recognition in aqueous media, *Nanoscale Res. Lett.* 4 (2009) 1230–1235.
- [26] N. Pradhan, A. Pal, T. Pal, Silver nanoparticle catalyzed reduction of aromatic nitro compounds, *Colloids Surf. A* 196 (2002) 247–257.
- [27] A. Henglein, Colloidal silver nanoparticles: photochemical preparation and interaction with O₂ CCl₄ and some metal ions, *Chem. Mater.* 10 (1998) 444–450.
- [28] S.H. Chen, K. Kimura, Water soluble silver nanoparticles functionalized with thiolate, *Chem. Lett.* 28 (1999) 1169–1170.
- [29] JCPDS Data File No. [87-0720].
- [30] M. Rusjan, M. Donnio, D. Guillon, F.D. Cukiernik, Liquid-crystalline materials based on rhodium carboxylate coordination polymers: synthesis, characterization and mesomorphic properties of tetra(alkoxybenzoato)dirhodium(II) complexes and their pyrazine adducts, *Chem. Mater.* 14 (2002) 1564–1575.
- [31] N. Wu, L. Fu, M. Su, M. Aslam, K.C. Wong, V.P. Dravid, Interaction of fatty acid monolayers with cobalt nanoparticles, *Nano Lett.* 4 (2004) 383–386.
- [32] R. Uppal, C.D. Incarvito, K.V. Lakshmi, A.M. Valentine, Aqueous spectroscopy and redox properties of carboxylate-bound titanium, *Inorg. Chem.* 45 (2006) 1795–1804.
- [33] T.V. Ramakrishna, G. Aravamudan, M. Vijayakumar, Spectrophotometric determination of mercury(II) as the ternary complex with rhodamine 6G and iodide, *Anal. Chim. Acta* 84 (1976) 369.
- [34] H.N. Kwan, G.S. Sergio, L.T. Lawrence, Mercury(II) adsorption from wastewaters using a thiol functional adsorbent, *Ind. Eng. Chem. Res.* 42 (2003) 1955.
- [35] T. Linnert, P. Mulvaney, A. Henglein, Surface chemistry of colloidal silver: surface plasmon damping by chemisorbed I⁻, SH⁻ and C₆H₅S⁻, *J. Phys. Chem.* 97 (1993) 679–682.
- [36] JCPDS Data File No. [27-0617].
- [37] M.S. Bootharaju, T. Pradeep, Uptake of toxic metal ions from water by naked and monolayer protected silver nanoparticles: An X-ray photoelectron spectroscopic investigation, *J. Phys. Chem. C* 114 (2010) 8328–8336.
- [38] J.F. Weaver, G.B. Hoflund, Surface characterization study of the thermal decomposition of AgO, *J. Phys. Chem.* 98 (1994) 8519–8524.
- [39] A. Mackova, V. Svorcik, P. Sajdl, Z. Stryhal, J. Pavlik, P. Malinsky, M. Slouf, RBS, XPS, and TEM study of metal and polymer interface modified by plasma treatment, *Vacuum* 82 (2008) 307–310.
- [40] D.G. Castner, K. Hinds, D.W. Grainger, X-ray photoelectron spectroscopy sulfur 2p study of organic thiol and disulfide binding interactions with gold surfaces, *Langmuir* 12 (1996) 5083–5086.
- [41] S. Biniak, M. Pakula, A. Swiatkowski, Influence of surface chemical structure of active carbon on its electrochemical behaviour in the presence of silver, *J. Appl. Electrochem.* 29 (1999) 481–487.